

Two-Body Local-Momentum Approximation of Spinless Particles Scattered by a (1+1)-D Woods–Saxon Barrier Potential

Karl-Erik Thylwe*

KTH-Mechanics, Royal Institute of Technology, S-10044 Stockholm, Sweden

(Received December 5, 2016; revised manuscript received December 22, 2016)

Abstract A local momentum (LM) approximation applicable to semi-relativistic two-body repulsive interactions is presented. It assumes negligible variations in the (vector-type) potential. A Woods–Saxon barrier with a rectangular-like shape is studied in some detail. The LM-approximation gives exact results within the semi-relativistic framework for rectangular barrier interactions in (1+1) dimensions. Further approximations of the local momentum approach leads to the two-body approximation of Ikhdaïr & Sever, known since the early 90’s as the spinless Salpeter equation approximating the Bethe–Salpeter equation. LM- and GS-results indicate significant two-body effects. Results obtained from the (single-mass) Dirac equation are similar for certain two-body mass combinations.

PACS numbers: 03.65.Nk, 03.65.Pm, 03.65.Xp, 11.80.-m

DOI: 10.1088/0253-6102/67/6/619

Key words: two-body effects, semi-relativistic, barrier transmission

1 Introduction

Recent research on relativistic two-body effects^[1–5] apply a semi-relativistic (SRQ) quantum approximation. With a related approximate approach by Ikhdaïr & Sever,^[1] two-body phenomena of bound and scattering states can be estimated with methods of non-relativistic quantum mechanics. Two-body effects appear as bound-state level shifts as well as scattering resonance shifts. Such two-body shifts are primarily due to special relativity. Shifts due to particle spins are ignored in the present semi-relativistic approach.

The approximation of the Bethe–Salpeter equation due to Ikhdaïr & Sever^[1] is a continuation of earlier ideas by Nickisch *et al.*,^[6] leading to a Schrödinger-like equation. It has been questioned by Lucha *et al.*^[2] for non-rigorous applications to bound-state calculations. Later research explains that the basic semi-relativistic quantum equation has exact solutions for step-like barriers to compare with, and that the approximation by Ikhdaïr & Sever accurately predicts transmission and reflection coefficients for (1+1)-D dynamics.^[5]

The idea by Ikhdaïr & Sever is different from other approaches, like those in Refs. [7–9]. Ikhdaïr & Sever directly quantize the energy-momentum invariant of special relativity. Required methods with this approach are familiar in non-relativistic quantum mechanics, as is obvious in recent applications assuming that relativistic contributions are small.^[3–4] Most of these applications focus on bound states in (1+1) dimensions (D) and in (1+3)-D. A couple of applications are related to scattering problems, see Refs. [4–5] for (1+1)-D barrier-type interaction potentials. However, early applications to bound and scattering states

do not discuss two-body effects, but rather analytic solution methods for specific potential shapes. The present local momentum (LM) approximation of the SRQ approach, also leading to a Schrödinger-like equation, is related to the exact SRQ treatment in Ref. [5], where a rectangular barrier was studied by matching linear plane-wave solutions.

One can think of the LM-approximation as an “adiabatic” approximation of a quantum-mechanical theory starting from a classical Hamiltonian from the special relativity. Such a semi-relativistic quantum theory presently ignores particle spin. The basic SRQ equation is still difficult to approach by standard numerical methods based on second-order ordinary differential equations (ODE). The main mathematical obstacle is the presence of square-root operators in the basic SRQ formulations. In subsequent sections the basic SRQ equation is simplified by further (adiabatic) approximations resulting in a second-order ODE. Once the Schrödinger-like equations are obtained, one can apply any standard numerical method of quantum mechanics. Here, the Milne’s numerical method is used, as explained elsewhere.^[11–13]

Two potential models are considered: The rectangular barrier, which allows exact numerical SRQ comparisons, is given by

$$V(x) = V_0, \quad -a < x < a, \quad \text{and} \quad V(x) = 0, \quad |x| \geq a. \quad (1)$$

Note that Alhaidari *et al.*^[14] studied transmission properties for a single fermion mass with scalar/vector-type rectangular barriers using Dirac theory.

The second model is an inverted Woods–Saxon poten-

*E-mail: kethylve@gmail.com

tial, a Woods–Saxon barrier, is given by

$$V(x) = \frac{V_0}{1 + \exp((|x| - a)/d)},$$

$$V_0 > 0, \quad -\infty < x < \infty, \quad (2)$$

where V_0 represents the potential strength, d is a length representing the “surface thickness” of nuclei, and a represents the effective size of nuclei. The parameters a and d are varied in the present study. Note that Thomson^[16] also studied transmission properties for a *single* fermion mass with scalar/vector-type Woods–Saxon barriers using Dirac theory.

From an earlier study of the rectangular (1+1) D barrier model,^[5] it became clear that the approximation by Ikhdair & Sever,^[1] here called the generalized Schrödinger (GS) approximation, is accurate with weak relativistic conditions on potential parameters. A critical parameter is the barrier strength V_0 , which causes extraordinary transmission behaviors for V_0 larger than m_2c^2 , where m_2 is the smaller of the two masses. For such values it is not obvious that the GS- and the LM approximations would agree for rectangular barriers, and even less obvious for smooth barriers like the Woods–Saxon barrier.

Section 2 describes the basic equations of the semi-relativistic quantum approach. The amplitude-phase approach is presented in Sec. 3. The particular LM approach is discussed in Sec. 4. Various approximations of the LM approach is presented in the same section, in particular the approximation of Ikhdair & Sever and the non-relativistic (Schrödinger) limit. Numerical and graphical results are shown in Sec. 5, and a conclusion is in Sec. 6.

2 Semi-Relativistic (SRQ) Two-Body Quantum Equation

The SRQ differential equation in the center-of-mass frame for relative motion of the masses m_1 and m_2 is linear, and given by^[5]

$$\mathcal{L}\Psi = \epsilon\Psi, \quad (3)$$

where ϵ is the dynamical energy (total energy minus rest-mass energies). The operator \mathcal{L} , including a relativistic (time-like) vector-type potential V , is given by

$$\mathcal{L} = \sqrt{m_1^2c^4 + \hat{p}^2c^2} - m_1c^2$$

$$+ \sqrt{m_2^2c^4 + \hat{p}^2c^2} - m_2c^2 + V. \quad (4)$$

The operator \mathcal{L} is linear, and far away from the interaction the solutions are plane waves ($\psi_{\pm k} = e^{\pm ikx}$) with an asymptotic wave number k . The plane waves satisfy Eq. (3),

$$\left(\sqrt{m_1^2c^4 + k^2\hbar^2c^2} + \sqrt{m_2^2c^4 + k^2\hbar^2c^2} \right) \psi_{\pm k}$$

$$= (mc^2 + \epsilon)\psi_{\pm k}, \quad (5)$$

where $m = m_1 + m_2$ is the total mass. An explicit relation between the wave number k and the energy ϵ is

$$k = \frac{1}{2\hbar c} \sqrt{\frac{\epsilon(2mc^2 + \epsilon)(2m_1c^2 + \epsilon)(2m_2c^2 + \epsilon)}{(mc^2 + \epsilon)^2}}, \quad (6)$$

which reduces to the non-relativistic (NR) expression

$$k_{\text{NR}} = \sqrt{\frac{2\mu\epsilon}{\hbar^2}}, \quad (7)$$

as $c \rightarrow +\infty$. The symbol μ is the reduced mass

$$\mu = \frac{m_1m_2}{m_1 + m_2}. \quad (8)$$

In the presence of a potential that vanishes as $|x| \rightarrow \infty$ the boundary conditions for the scattering wave function Ψ can be written as

$$\Psi \sim t \exp(-ikx), \quad x \rightarrow -\infty, \quad (9)$$

$$\Psi \sim \exp(-ikx) + r \exp(ikx), \quad x \rightarrow +\infty, \quad (10)$$

where t and r are the transmission and reflection amplitudes, respectively. Expressions for the transmission and reflection coefficients are:

$$T = |t|^2, \quad (11)$$

$$R = |r|^2. \quad (12)$$

These quantities are computed with the aid of Secs. 3 and 4 for the rectangular and the Woods–Saxon potentials by the amplitude-phase method. Results are presented in Sec. 5 and further discussed in Sec. 6.

3 Schrödinger-Like Equations and the Amplitude-Phase Method

In this study the relevant approximations of the SRQ equation (3) are defined by Schrödinger-like equations; see the subsequent sections. Hence, the approximate solutions are obtained from

$$\frac{d^2}{dx^2}\Psi + K^2(x)\Psi = 0, \quad (13)$$

with a variable coefficient function $K^2(x)$, and one can apply standard numerical method of quantum mechanics to solve the barrier problem. In the present study the amplitude-phase method is applied.^[11–12] It is based on two amplitude-phase representations, left(L)- and right(R) representations, of fundamental solutions satisfying Eq. (13). These are

$$\Psi_{L,R}^{(\pm)}(x) = A_{L,R}(x) \exp(\pm i\phi_{L,R}(x)), \quad (14)$$

$$\frac{d}{dx}\phi_{L,R}(x) = A_{L,R}^{-2}(x), \quad (15)$$

where Eq. (15) is an auxiliary relation ensuring the Wronskian determinant of the two (\pm)-solutions (14) being constant. This condition can be imposed since the number of symbols is doubled. Inserting Eq. (14) into the Schrödinger-like equation (13), one obtains a nonlinear Milne equation^[12]

$$\frac{d^2}{dx^2}A_{L,R} + K^2(x)A_{L,R} = A_{L,R}^{-3}. \quad (16)$$

From the two L, R -representations (14) and (15) one defines fundamental matrix solutions

$$\Psi_{L,R} = \begin{pmatrix} \Psi_{L,R}^{(+)} & \Psi_{L,R}^{(-)} \\ \Psi'_{L,R}^{(+)} & \Psi'_{L,R}^{(-)} \end{pmatrix}, \quad (17)$$

where a prime, $'$, indicates a derivative with respect to x . The fundamental solutions are matched at the origin $x = 0$ as described in Ref. [11]. The resulting L, R -connection is

$$\Psi_L(x) = \Psi_R(x)\mathbf{M}, \quad (18)$$

where \mathbf{M} is a complex-valued 2×2 matrix, given by

$$\mathbf{M} = \frac{1}{2} \begin{pmatrix} -iP + Q + Q^{-1} & -iP + Q - Q^{-1} \\ iP + Q - Q^{-1} & iP + Q + Q^{-1} \end{pmatrix}, \quad (19)$$

with

$$P = A'_L(0)A_R(0) - A'_R(0)A_L(0), \quad (20)$$

$$Q = \frac{A_L(0)}{A_R(0)}. \quad (21)$$

In the present case the barrier is symmetric with respect to $x = 0$, and one can use amplitude solutions of Eq. (16) satisfying

$$A_L(-x) = A_R(x), \quad A'_L(-x) = -A'_R(x). \quad (22)$$

Hence, the matrix (19) can be written directly in terms of amplitude values, i.e.

$$\mathbf{M} = \begin{pmatrix} iA'_R(0)A_R(0) + 1 & iA'_R(0)A_R(0) \\ -iA'_R(0)A_R(0) & -iA'_R(0)A_R(0) + 1 \end{pmatrix}. \quad (23)$$

The transmission- and reflection coefficients are obtained as

$$T = \frac{1}{M_{22}M_{22}^*}, \quad (24)$$

$$R = \frac{M_{12}M_{12}^*}{M_{22}M_{22}^*}, \quad (25)$$

and by direct evaluations of the \mathbf{M} -matrix elements the resulting expressions become

$$T = \{1 + [A'_R(0)A_R(0)]^2\}^{-1}, \quad \text{and } R = 1 - T. \quad (26)$$

The reflection symmetry of the present potential implies that Eq. (26) can be used. Hence, only one of the amplitude functions, say $A_R(x)$, is to be integrated. For scattering solutions the Milne equation (16) is integrated from initial conditions at any $x_{\text{init}} \gg a$, where a is the range parameter, with

$$\begin{aligned} A_R(x_{\text{init}}) &= K^{-1/2}(+\infty), \\ A'_R(x_{\text{init}}) &= 0, \quad x_{\text{init}} \rightarrow +\infty. \end{aligned} \quad (27)$$

The constant $K(+\infty) > 0$ is the relevant asymptotic wave number. The integration terminates at $x = 0$ and the

values $A_R(0), A'_R(0)$ are inserted into Eq. (26). Results depend very little on position of $x_{\text{init}} \gg a$ if the tail of the potential vanishes exponentially. For the Woods–Saxon potential $x_{\text{init}} \approx 10a$ is used. The numerical tolerance of the integrator is $\approx 10^{-7}$.

The initial (boundary) conditions (27) are taken from an exact constant solution of the nonlinear equation (16) as $x \rightarrow +\infty$. The exact wave number in Eq. (6) is the relevant one for the local-momentum (LM) approximation presented in the subsequent section.

4 Local-Momentum (LM) Approximation

The aim of the LM-approximation is to obtain a Schrödinger-type differential equation instead of Eq. (3), and, thereby revealing a relation to the generalized Schrödinger (GS) approximation of Ikhdaïr & Severe.^[1]

The key observation motivating a “local-momentum” approximation is this: the plane-wave solutions $\psi_{\pm k} = e^{\pm ikx}$ satisfy the original SRQ equation (3) *as well as* the second-order ODE:

$$\hat{p}^2 \psi_{\pm k} = \hbar^2 k^2 \psi_{\pm k}, \quad (V = 0), \quad (28)$$

where k is defined in Eq. (6). Hence, for a vanishing potential V , Eq. (3) can be replaced by Eq. (28), which appears as a “generating second-order differential equation” for Eq. (3).

An algebraic manipulation with the same resulting Eq. (28) is possible by assuming V being constant in Eq. (3) and treating the operator \hat{p}^2 as a c -number or a *local* function. The operator status of \hat{p}^2 is subsequently retained after the completed algebra, and the solution is exact.

The main approximation of such algebraic manipulations is that the potential has no derivatives in connected intervals of the x -axis. The solutions are linear and can be rigorously fitted at each discontinuity of the x -axis.

To generalize this situation one can instead of a discontinuity think of a smooth transition between two (almost) constant values of V . The rectangular-shaped Woods–Saxon barrier is the potential model chosen for this purpose. Here it is proposed that a discontinuity can be replaced by a small (surface thickness) region with possibly large derivatives of the potential.

By heuristically assuming the potential V being piecewise constant with sufficiently small transition regions, one obtains an equation (13) with $K^2(x)$ replaced by

$$K_{\text{LM}}^2(x) = \frac{1}{4\hbar^2 c^2} \left[\frac{(\epsilon - V)(2mc^2 + \epsilon - V)(2m_1 c^2 + \epsilon - V)(2m_2 c^2 + \epsilon - V)}{(mc^2 + \epsilon - V)^2} \right], \quad (29)$$

or equivalently

$$K_{\text{LM}}^2(x) = \frac{2m}{\hbar^2} \left[(\epsilon - V) \left(\frac{m_1}{m} + \frac{\epsilon - V}{2mc^2} \right) \left(\frac{m_2}{m} + \frac{\epsilon - V}{2mc^2} \right) \frac{(1 + (\epsilon - V)/2mc^2)}{(1 + (\epsilon - V)/mc^2)^2} \right]. \quad (30)$$

Contributions from derivatives of the potential V are ignored in this study.

It is interesting to approximate the coefficient $K_{\text{LM}}^2(x)$ in different limiting directions. Five particular cases are:

- The equal-mass situation:

$$K_{\text{LM}m_1=m_2}^2(x) = \frac{m}{2\hbar^2} \left[(\epsilon - V) \left(1 + \frac{\epsilon - V}{2mc^2} \right) \right], \quad m = 2m_1 = 2m_2 = 4\mu; \quad (31)$$

- The extreme light-heavy situation:

$$K_{\text{LM}m_2=0}^2(x) = \frac{1}{\hbar^2 c^2} \left[(\epsilon - V)^2 \frac{(1 + (\epsilon - V)/2mc^2)^2}{(1 + (\epsilon - V)/mc^2)^2} \right], \quad m = m_1; \quad (32)$$

- The weak, relativistic situation:

$$K_{\text{GS}}^2(x) = K_{\text{LM}c \rightarrow \infty}^2(x) = \frac{2\mu}{\hbar^2} (\epsilon - V) + \left(\frac{m - 3\mu}{m} \right) \frac{1}{\hbar^2 c^2} (\epsilon - V)^2; \quad (\text{GS}) \quad (33)$$

- The non-relativistic situation:

$$K_{\text{NR}}^2(x) = K_{\text{LM}c=\infty}^2(x) = \frac{2m}{\hbar^2} \left[(\epsilon - V) \frac{m_1 m_2}{m^2} \right] = \frac{2\mu}{\hbar^2} (\epsilon - V); \quad (\text{NR}) \quad (34)$$

- The weak potential situation:

$$K_{\text{LM}V \rightarrow 0}^2(x) = \frac{1}{4\hbar^2 c^2} [B_0 - B_1 V + B_2 V^2], \quad (35)$$

with expansion parameters

$$B_0 = \frac{\epsilon(2mc^2 + \epsilon)(2m_1c^2 + \epsilon)(2m_2c^2 + \epsilon)}{(mc^2 + \epsilon)^2},$$

$$B_1 = 2 \left[mc^2 + \epsilon - \frac{m_1^2 c^4 + m_2^2 c^4}{mc^2 + \epsilon} \right] \left[1 - \frac{m_1^2 c^4 - m_2^2 c^4}{(mc^2 + \epsilon)^2} \right],$$

$$B_2 = 1 + \frac{3m^2 c^4 (m_1 - m_2)^2 c^4}{(mc^2 + \epsilon)^4}.$$

Note that the second case (32) does not imply “a single particle scattering in a potential V ”. Instead, one actually has a two-body scattering case here, where one of the particles is massless like a photon. Note also that the third case (33) is similar to the Schrödinger-type coefficient function of Ikhdaïr & Sever-approximation.^[1] In this approximation the two-body mass index satisfies

$$\frac{1}{4}(\text{equal masses}) \leq \left(\frac{m - 3\mu}{m} \right) < 1 \text{ (light-heavy masses limit)}. \quad (36)$$

Two of the above coefficient approximations, Eqs. (33) and (34), are applied numerically and included for comparisons with Eq. (30) in Tables 1–4.

5 Results for the (1+1) D Rectangular and Woods–Saxon Barriers

The rectangular barrier case has analytic solutions of the transmission and reflection coefficients and allows exact semi-relativistic results.^[5] The LM approximation becomes exact and the GS approximation turns out to be surprisingly accurate, although the GS-wave numbers are not particularly accurate in general.^[5] The LM- and GS approximations suite the amplitude-phase method well.^[11]

Both approximations result in differential equations of the Schrödinger type. Numerical values of the transmission coefficient reveals possible oscillatory behaviors at very low scattering energies and strongly repulsive barriers (see below). These are spectacular two-body effects that at the moment should be seen as hypothetical, but

inherent to the “semi-relativistic” approach. For such parameter values (strong, repulsive barriers) the fundamentals of the semi-relativistic approach are questionable.

Table 1 (Color online) Two-body transmission coefficients T for the rectangular barrier with parameters $V_0 = 2\mu$, $a = 3$, $m_1 = 100\mu$, $d = 0$, and varying scattering energies ϵ . Symbols in the table of the calculated transmission coefficient: T (exact analytic), T_{LM} (numerical LM-calculations), T_{GS} (Ikhdaïr & Sever), and T_{NR} (non-relativistic).

ϵ/V_0	T_{exact}	T_{LM}	T_{GS}	T_{NR}
1.2	0.730 51	0.730 51	0.729 37	0.603 88
1.4	0.815 73	0.815 73	0.818 42	0.706 26
1.6	0.724 83	0.724 83	0.728 35	0.995 67
1.8	0.702 39	0.702 39	0.699 61	0.860 64
2.0	0.804 85	0.804 85	0.786 49	0.965 26

For rectangular barriers the predictive power of two-body effects of the GS approximation can be rigorously estimated; see Table 1. When the rectangular barrier becomes a smooth function of x , both LM- and GS-approaches are approximate. For the Woods–Saxon barrier one can still study how the LM- and GS-approximations relate to each other as the surface thickness d of the Woods–Saxon barrier increases. One can also study the relation to Dirac theory for a single fermion in a potential field.

5.1 Rectangular Barrier

In Ref. [5] it was shown that transmission properties for the light-heavy mass systems differ the most compared to non-relativistic calculations. Therefore the mass parameters in Table 1 (rectangular potential) are chosen as $m_1 = 100\mu$ and $\mu = 1$. The potential strength is $V_0 = 2\mu c^2$ in Table 1 (rectangular potential), which is close to a critical value for which the waves become oscillatory in an extreme sub-barrier energy region (see Figs. 2 and 3). Furthermore, the barrier range is chosen as $a = 3$

in Table 1.

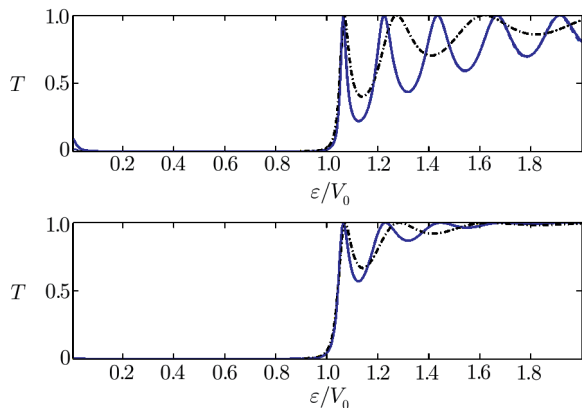


Fig. 1 (Color online) Transmission coefficients for sharp (upper subplot) and smooth (lower subplot) Woods–Saxon barrier as function of ϵ/V_0 . Specific potential parameters are: $V_0 = 2\mu$, $\mu = 1$, $m_1 = 100\mu$, $a = 3$, with $d = 0.01$ (upper subplot) and $d = 0.2$ (lower subplot). The LM- and GS-approximations are represented by the same continuous curves and the non-relativistic (NR) approximation by dashed-dotted curves.

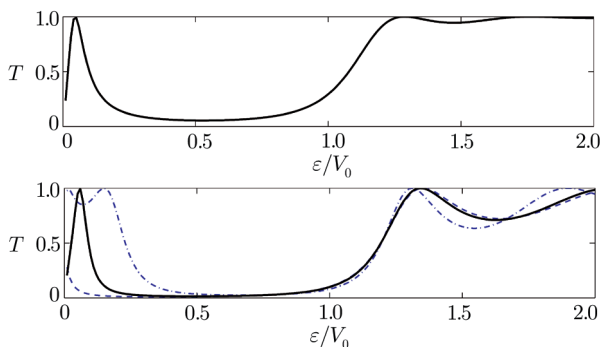


Fig. 2 (Color online) Dirac (upper subplot) and LM (lower subplot) computations of T for a Woods–Saxon barrier as function of ϵ/V_0 , where $d = 0.01$, $V_0 = 3\mu c^2$, $\mu = 1$, $a = 1$. Upper plot corresponds to results from Dirac computations with the single-particle mass μ . The lower subplot corresponds to three cases of two-body SRQ computations. Black continuous curve represents $m_1 = 3.7\mu$, while blue dashed-dotted curve corresponds to $m_1 = 100\mu$ and blue dashed curve corresponds to $m_1 = 3\mu$.

Table 1 shows that the numerical local momentum approach agrees with the analytic exact results for the transmission coefficient, as expected. In Ref. [5] the generalized Schrödinger (GS) equation by Ikhdaïr & Sever^[1] turned out to be accurate for moderate potential strengths. This accuracy is valid also in the present cases, in particular for the sub-barrier energy regions (not shown). However, the relative accuracy is gradually lost to between $\approx 0.2\%$ and $\approx 2\%$ in the super-barrier energy region (Table 1), where the transmission coefficient is oscillatory; see also Fig. 1 for the Woods–Saxon potential. The non-relativistic approximation (T_{NR}) is reasonably accurate only in the sub-

barrier energy region, and behaves similar to the dashed-dotted lines in Fig. 1.

5.2 Woods–Saxon Barrier

Hence, the numerical results show that the GS approximation is accurate even at the strong potential barrier with $V_0 = 2\mu c^2$, where $\mu = 1$. This is twice the barrier height considered in Ref. [5]. The only remarkable deviation between LM and GS results is at very low scattering energies. This difference is indicated also in the upper subplot (small d) of Fig. 1 for the Woods–Saxon barrier. It corresponds to the strange two-body effect of the SRQ equation mentioned earlier, but apparently exists for smooth (but sharp) barriers. An increase of the potential strength to $V_0 > 2\mu c^2$ results in effects similar to single-mass phenomena discussed recently within the Dirac framework^[14] (see Fig. 2).

Tables 2–4 show the transmission coefficient for the same potential strength V_0 and size a as in Table 1, but with variable surface thickness $d = 0.01, 0.2$, and 1 .

Table 2 Two-body transmission coefficients T for the Wood–Saxon barrier with parameters $V_0 = 2\mu$, $a = 3$, $d = 0.01$, $m_1 = 100\mu$, and varying scattering energies ϵ . Symbols in the table of the calculated transmission coefficient: T_{LM} (numerical LM-calculations), T_{GS} (Ikhdaïr & Sever), and T_{NR} (non-relativistic).

ϵ/V_0	T_{LM}	T_{GS}	T_{NR}
1.2	0.738 72	0.737 84	0.604 75
1.4	0.822 79	0.825 75	0.707 24
1.6	0.730 98	0.734 84	0.995 69
1.8	0.706 38	0.703 98	0.861 46
2.0	0.805 70	0.787 78	0.965 52

For scattering energies near the barrier top energies, e.g. $0.9V_0 < \epsilon < 1.1V_0$ in Fig. 1, there are striking agreements between all approximations considered. For the sharp case ($d = 0.01$) in the upper subplot in Fig. 1, relativistic differences occur at very low (non-relativistic) scattering energies and different masses. These are related to situations in the Dirac approach for single masses discussed by Alhaidari *et al.*^[14] However, this difference disappears for $d = 0.1$. Differences with respect to non-relativistic results occur more generally at energies significantly above the barrier-top energies (see Tables 2–4). However, the GS- and LM results are indistinguishable in Fig. 1.

Table 2 studies the transmission coefficient of a Woods–Saxon barrier with a sharp surface ($d = 0.01$). The results are approximately the same as in Table 1 for the rectangular barrier. In the upper subplot of Fig. 1 ($d = 0.01$), corresponding to Table 2, the continuous curve represents LM- and GS computations. In contrast, the non-relativistic (dashed-dotted) curve in Fig. 1 (upper subplot) deviates more and more from the others with increasing scattering energy.

Table 3 Two-body transmission coefficients T for the inverted Wood–Saxon barrier with parameters $V_0 = 2\mu$, $a = 3$, $d = 0.2$, $m_1 = 100\mu$, and varying scattering energies ϵ . Symbols in the table of the calculated transmission coefficient: T_{LM} , T_{GS} (Ikhdaïr & Sever), and T_{NR} (non-relativistic).

ϵ/V_0	T_{LM}	T_{GS}	T_{NR}
1.2	0.920 55	0.921 37	0.805 29
1.4	0.967 25	0.968 19	0.922 19
1.6	0.976 85	0.977 46	0.996 46
1.8	0.990 78	0.990 71	0.983 35
2.0	0.998 69	0.998 47	0.994 83

Table 3 and the lower subplot of Fig. 1 show the transmission coefficient of a Woods–Saxon barrier with a less sharp surface ($d = 0.2$). The agreement between GS- and LM results is even better. The oscillation amplitudes of the transmission coefficient have become smaller. Table 4 shows results from a non-rectangular barrier with surface thickness $d = 1$. The table shows a complete agreement between GS- and LM results. Non-relativistic results are also approximately the same. The approximations used here tend to be more similar as the surface thickness increases.

Table 4 Two-body transmission coefficients T for the inverted Wood–Saxon barrier with parameters $V_0 = 2\mu$, $a = 3$, $d = 1$, $m_1 = 100\mu$, and varying scattering energies ϵ . Symbols in the table of the calculated transmission coefficient: T_{LM} (numerical LM-calculations), T_{GS} (Ikhdaïr & Sever), and T_{NR} (non-relativistic).

ϵ/V_0	T_{LM}	T_{GS}	T_{NR}
1.2	0.997 54	0.997 54	0.997 74
1.4	0.999 62	0.999 62	0.999 71
1.6	0.999 87	0.999 87	0.999 89
1.8	0.999 94	0.999 94	0.999 95
2.0	0.999 97	0.999 97	0.999 97

As a final study, the Woods–Saxon potential is used to compare SRQ results with the results of the (single-mass) Dirac theory as the surface thickness is $d = 0.01$ (see Refs. [14–15]). For such potentials there are speculative investigations about zero-momentum resonances and low-energy ($\epsilon \approx 0$) total transmissions for very large barriers.

The upper (Dirac) and lower (LM) subplots in Fig. 2 show the transmission coefficient corresponding to the same reduced masses and potential parameters, but the methods are different. The Woods–Saxon parameters are $d = 0.01$, $V_0 = 3\mu c^2$, $\mu = 1$, $a = 1$. Note that the potential strength is much stronger than that in Fig. 1. The Dirac mass in the upper subplot is μ . The individual masses in the lower subplot are defined by μ and the large mass $m_1 = 3\mu, 3.7\mu$, and $m_1 = 100\mu$. The upper subplot is the result from the Dirac equation in

(1+1) relativistic dimensions.^[14–16] In the LM approximation $m_1 = 100\mu$ (dashed-dotted curve), $m_1 = 3.7\mu$ (solid curve), and $m_1 = 3\mu$ (dashed curve). The best low-energy similarity of the transmission coefficients of the upper and lower subplots in Fig. 2 is for $m_1 = 3.7\mu$ (solid curve) in this case. The other mass combinations show completely different low-energy dependences. For equal masses ($m_1 = 2\mu$, not shown) large transmissions have not been found in the present investigation.

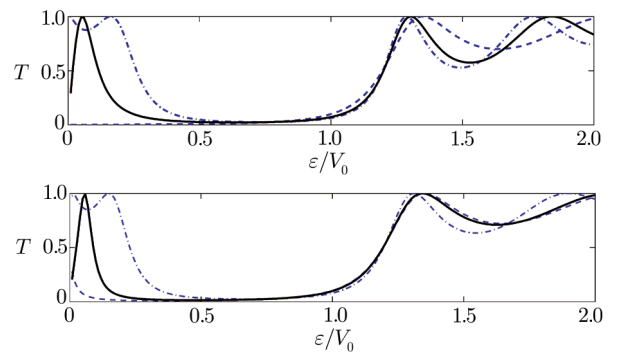


Fig. 3 GS (upper subplot) and LM (lower subplot) computations of T as function of ϵ/V_0 for three mass combinations each, where $d = 0.01$, $V_0 = 3\mu c^2$, $\mu = 1$, $a = 1$. The continuous (black) curves are nice fits to the Dirac results from Fig. 2. The “nice-fit” GS curve corresponds to $m_1 = 11\mu$, and the “nice-fit” LM curve corresponds to $m_1 = 3.7\mu$.

Figure 3 compares GS- and LM-calculations for the Woods–Saxon parameters $d = 0.01$, $V_0 = 3\mu c^2$, $\mu = 1$, $a = 1$. Of three mass combinations each, nice fits to Dirac results are obtained for $m_1 = 11\mu$ (upper subplot, solid curve) from the GS equation, and $m_1 = 3.7\mu$ (lower subplot, solid curve also in Fig. 2) from the LM equation. For $m_1 = 100\mu$ (dashed-dotted curves) both GS- and LM-results show double peaks at low-energies. For $m_1 = 3\mu$ (dashed curves) the GS-method (upper subplot) predicts no transmission peak at threshold energies, while the LM-method predicts some enhanced transmission.

Note that the Dirac results agree approximately with a light-heavy mass (almost single-mass) combination (GS and LM) only at higher energies, above the potential top energy.

6 Conclusion

The local momentum (LM) and the generalized Schrödinger (GS) approximations are numerically compared. Both approximations assume negligible variations in the potential. A Woods–Saxon barrier with parameters close to a rectangular shape is studied in some detail. The LM-approximation provides exact results within the semi-relativistic two-body framework for rectangular barrier interactions in (1+1) dimensions, but the GS-approximation provides almost the same results.

This study suggests that GS/LM-approximations are numerically similar for weak potential strengths and a wide range of scattering energies. For very strong interactions, the study shows similarities between LM/GS and Dirac results at energies above the barrier maximum. However, the Dirac-“best-fit” (LM/GS) mass combinations are not the same.

The surface thickness parameter d seems to make LM, GS and non-relativistic results numerically closer to each other as d increases. This is observed in Table 4 for the over-barrier energy region ($\epsilon > V_0$), where $T \sim 1$ (with very small oscillations).

For barrier widths comparable with the Compton length ($a \approx 1$) the Dirac results do not agree with re-

sults from SRQ “light-heavy” mass combinations. The strongest difference between the Dirac and SRQ results is for equal masses, in which case SRQ results do not indicate any tunneling at low scattering energies, and therefore no large low-energy transmissions.

“Super-strong” interactions for $V_0 - \epsilon > 2\mu c^2$ seem speculative and not fully understood. The more important to compare these results with quantum field theory. Single-particle Dirac results, pointed out by Alhaidari *et al.*,^[14] Thomson^[15] and others, indicate total transmission at low (non-relativistic) scattering energies. For equal masses the present study indicates non-existence of large low-energy transmissions.

References

- [1] S. M. Ikhdair and R. Sever, IC/92/186 (INTERNAL REPORT) (1994); S. M. Ikhdair and R. Sever, *Int. J. Mod. Phys. E* **17** (2008) 1107; S. M. Ikhdair and R. Sever, *Int. J. Mod. Phys. A* **20** (2005) 16509.
- [2] W. Lucha and F. F. Schöberl, *Int. J. Mod. Phys. A* **17** (2002) 2233; W. Lucha and F. F. Schöberl, *Int. J. Mod. Phys. A* **15** (2000) 3221; W. Lucha and F. F. Schöberl, *Int. J. Mod. Phys. A* **14** (1999) 2309; W. Lucha and F. F. Schöberl, *Fizika B* **8** (1999) 193; W. Lucha and F. F. Schöberl, *Phys. Rev. A* **60** (1999) 5091; W. Lucha and F. F. Schöberl, *Phys. Rev. A* **54** (1996) 3790; W. Lucha and F. F. Schöberl, *Phys. Rev. D* **50** (1994) 5443; W. Lucha and F. F. Schöberl, *Phys. Rev. D* **50** (1994) 5443.
- [3] S. Hassanabadi, M. Ghominejada, S. Zarrinkamar, and H. Hassanabadi, *Chin. Phys. B* **22** (2013) 060303; S. Hassanabadi and A. A. Rajabi, *Mod. Phys. Lett. A* **27** (2012) 1250057; S. Zarrinkamar, A. A. Rajabi, H. Hassanabadi, and H. Rahimov, *Phys. Scr.* **84** (2011) 065008; S. Zarrinkamar, A. A. Rajabi, and H. Hassanabadi, *Few-Body Sys.* **52** (2011) 165.
- [4] S. Hassanabadi, M. Ghominejada, and K. E. Thylwe, *Commun. Theor. Phys.* **63** (2015) 423.
- [5] K. E. Thylwe, O. J. Oluwadare, and K. J. Oyewumi, *Commun. Theor. Phys.* **66** (2016) 389.
- [6] I. J. Nickisch, B. Durand, and L. Durand, *Phys. Rev. D* **25** (1982) 2312; I. J. Nickisch, B. Durand, and L. Durand, *Phys. Rev. D* **30** (1984) 1904.
- [7] S. J. Wallace, *Phys. Rev. Lett.* **87** (2001) 180401.
- [8] J. Bijtebier and J. Broekaert, *Nuovo Cimento A* **105** (1992) 351.
- [9] R. Arshansky and L. P. Horwitz, *J. Math. Phys.* **30** (1989) 213.
- [10] N. F. Mott and H. S. W. Massey, *The Theory of Atomic Collisions*, Oxford University Press, Cambridge, Ch. 2 (1965).
- [11] K. E. Thylwe, *J. Phys. A: Math. Gen.* **38** (2005) 235.
- [12] W. E. Milne, *Phys. Rev.* **35** (1930) 863; H. A. Wilson, *Phys. Rev.* **35** (1930) 948; H. A. Young, *Phys. Rev.* **38** (1931) 1612; H. A. Young, *Phys. Rev.* **39** (1932) 455; J. A. Wheeler, *Phys. Rev.* **52** (1937) 1123.
- [13] H. J. Korsch and H. Laurent, *J. Phys. B* **14** (1981) 4213.
- [14] A. D. Alhaidari, H. Bahlouli, Y. Benabderahmane, and A. Jellal, *Phys. Rev. A* **86** (2012) 052113.
- [15] M. J. Thomson and B. H. J. McKellar, *Am. J. Phys.* **59** (1991) 340.